

Friction and mobility of carbon nanoparticles on a graphene sheet

Alexander V. Savin^{1,2,*}

¹*Semenov Institute of Chemical Physics, Russian Academy of Sciences, Moscow 119991, Russia*

²*Plekhanov Russian University of Economics, Moscow 117997, Russia*

It is shown using the method of molecular dynamics that the motion of carbon nanoparticles (rectangular graphene flakes, spherical fullerenes of size $L < 10$ nm) on the surface of a thermalized graphene sheet lying on a flat substrate can be described as the motion of particles in a viscous medium with a constant coefficient of friction, the value of which depends on the temperature and particle size. It has been shown that there are two types of effective friction: diffusion and ballistic. In ballistic regime of motion (at velocities $v > 100$ m/s), deceleration occurs due to the interaction of moving nanoparticles with thermal out-of-plane bending vibrations of a graphene sheet. Because of this, with the increasing temperature, the coefficient of friction monotonically increases. In the diffusion regime of motion (at $v < 10$ m/s), friction arises due to the need for the particle to overcome local energy barriers, therefore it decreases with increasing temperature. The difference between ballistic and diffusion friction is most pronounced at low temperatures, since the mobility of nanoparticles in the ballistic regime of motion decreases with increasing temperature, while in the diffusion regime it monotonously increases. It is shown that the presence of a normal force pressing the nanoparticle to the substrate leads to an increase in its friction with the substrate.

I. INTRODUCTION

Two-dimensional layered materials such as graphene (G, hexagonal boron nitride (hBN), molybdenum disulfide (MoS₂) and tungsten disulfide (WS₂) are of great interest because of their unique electronic [1–3] and mechanical [4–7] properties. Due to the very low friction of the layers, these materials can be used as highly efficient dry lubricants [8–14]. Recently, increased attention has been paid to heterogeneous layered materials that can exhibit various new physical properties compared to their homogeneous analogues [15–17]. Thus, it was shown that the use of G/h-BN heterostructures makes it possible to obtain the necessary electronic properties [18, 19], as well as significantly reduce the friction between the layers [20].

An important task for nano- and micro-sized mechanical devices is to reduce friction as much as possible [21]. Standard lubrication schemes stop working at such sizes, so it is necessary here to switch from liquid to dry lubricant, associated with the sliding of flat molecular layers. This approach, first theoretically proposed several decades ago [22], allowed to achieve extremely low coefficients of friction [23–25]. The use of two-dimensional materials, such as graphene and hexagonal boron nitride h-BN [26], makes it possible to achieve extremely low friction. Layered structures made of these materials can have super-slip layers [15, 20, 27].

The use of 2D layered structures requires a fundamental understanding of the mechanisms of the appearance of the friction force at the atomic level. To date, this mechanism has been well studied only for slow "diffusion" motion of layers (at velocities $v < 10$ m/s) [20, 27–30]. Modeling of the motion of nanoparticles (clusters Au₄₅₉ [31], fullerene molecules C₆₀ [32]) on the surface of

a graphene sheet showed that at velocities $v > 100$ m/s there is another "ballistic" regime of friction.

The goal of this paper is to explain the mechanisms of the occurrence of friction forces in the ballistic regime of nanoparticles motion. For this purpose, the motion of carbon nanoparticles (rectangular graphene flakes and spherical fullerene molecules) along a thermalized graphene nanoribbon lying on a flat substrate will be simulated. It will be shown that at high velocities of motion, friction has a "wave" origin. Here, the deceleration of motion occurs due to the interaction of the moving nanoparticle with thermal out-of-plane bending vibrations of a graphene sheet (the greater are the vibrations, the higher is the friction). Therefore, in ballistic motion, unlike standard friction scenarios [29], the coefficient of friction monotonically increases with increasing temperature.

The paper is structured as follows: the section II describes the full-atomic model, which is further used to simulate the motion of carbon nanoparticles on a thermalized graphene sheet lying on a flat substrate. In section III, the deceleration of the free motion of nanoparticles as a result of their interaction with the sheet are simulated. The coefficient of effective friction is determined and the mechanism of its occurrence is analyzed. In section IV, the motion of nanoparticles under the action of a constant force directed parallel to the substrate surface is modeled. The mobility of nanoparticles in diffusion and ballistic regimes of motion is analyzed. In section V, the empirical Amonton-Coulomb law is verified for nanoparticles. The influence of the normal load (of the force pressing the nanoparticle to the substrate) on the value of friction is simulated. The analysis of the results and concluding remarks are given in section VI.

*asavin@center.chph.ras.ru

II. MODEL

Let us simulate the movement of rectangular graphene flakes (RGF) and spherical fullerenes (SF) along a graphene sheet lying on a flat substrate – see Fig. 1. As a graphene sheet, we will use graphene nanoribbon (GNR) of size $103.0 \times 19.0 \text{ nm}^2$ lying in the xy plane (the x axis is directed along the zigzag direction) and consisting of $N_1 = 75598$ carbon atoms. In realistic cases, the edges of the graphene nanoribbon and rectangular flakes are always chemically modified. For simplicity, we assume that the hydrogen atoms are attached to each edge carbon atom. In our numerical simulations, we take this into account by a change of the mass of the edge atoms. We assume that the edge carbon atoms have the mass $M_1 = 13m_p$, while all other internal carbon atoms have the mass $M_0 = 12m_p$, where $m_p = 1.6601 \times 10^{-27} \text{ kg}$ is the proton mass.

Hamiltonian of the RGF(SF)/GNR molecular system consisting of $N = N_1 + N_2$ carbon atoms (N_2 – number of atoms of RGF (SF)) can be presented in the form,

$$H = \sum_{n=1}^N \left[\frac{1}{2} M_n (\dot{\mathbf{u}}_n, \dot{\mathbf{u}}_n) + P_n + W(\mathbf{u}_n) \right] + \sum_{n=1}^{N_1} \sum_{k=N_1+1}^N V(r_{nk}), \quad (1)$$

where n is the number of carbon atom, M_n is the mass of the n th atom (for internal atoms $M_n = 12m_p$ and $M_n = 13m_p$ for the edge atoms), $\mathbf{u}_n = (x_n(t), y_n(t), z_n(t))$ is the three-dimensional vector describing the position of n th atom at the time t , distance $r_{nk} = |\mathbf{u}_n - \mathbf{u}_k|$. The term P_n describes the interaction of the carbon atom with the index n with the neighboring atoms. The potential depends on variations in bond length, bond angles, and dihedral angles between the planes formed by three neighboring carbon atoms and it can be written in the form

$$P = \sum_{\Omega_1} U_1 + \sum_{\Omega_2} U_2 + \sum_{\Omega_3} U_3 + \sum_{\Omega_4} U_4 + \sum_{\Omega_5} U_5, \quad (2)$$

where Ω_i , with $i = 1, 2, 3, 4, 5$, are the sets of configurations including all interactions of neighbors. These sets only need to contain configurations of the atoms shown in Fig. 2, including their rotated and mirrored versions.

Potential $U_1(\mathbf{u}_n, \mathbf{u}_m)$ describes the deformation energy due to a direct interaction between pairs of atoms with the indexes n and m , as shown in Fig. 2(a). The potential $U_2(\mathbf{u}_n, \mathbf{u}_m, \mathbf{u}_k)$ describes the deformation energy of the angle between the valence bonds $\mathbf{u}_n \mathbf{u}_m$, and $\mathbf{u}_m \mathbf{u}_k$, see Fig. 2(b). Potentials $U_i(\mathbf{u}_n, \mathbf{u}_m, \mathbf{u}_k, \mathbf{u}_l)$, $i = 3, 4$, and 5 , describe the deformation energy associated with a change in the angle between the planes $\mathbf{u}_n \mathbf{u}_m \mathbf{u}_k$ and $\mathbf{u}_m \mathbf{u}_n \mathbf{u}_k$, as shown in Figs. 2(c)–(e).

We use the potentials employed in the modeling of the dynamics of large polymer macromolecules [33, 34] for the valence bond coupling,

$$U_1(\mathbf{u}_1, \mathbf{u}_2) = \epsilon_1 \{ \exp[-\alpha_0(\rho - \rho_0)] - 1 \}^2, \quad \rho = |\mathbf{u}_2 - \mathbf{u}_1|, \quad (3)$$

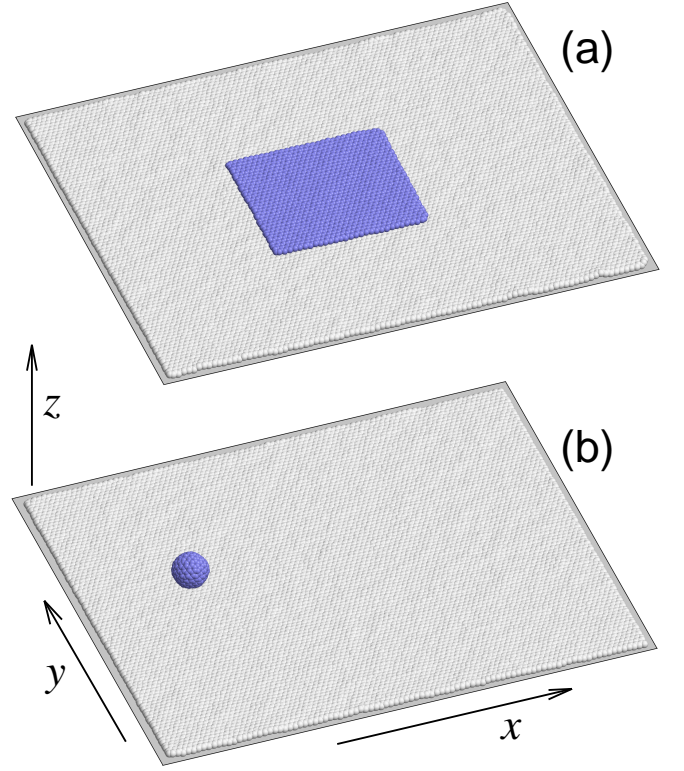


FIG. 1: Simulation of the motion of (a) a rectangular graphene flake (RGF) of size $7.245 \times 6.665 \text{ nm}^2$, consisting of $N_2 = 1918$ carbon atoms, and (b) spherical fullerene (SF) C_{240} ($N_2 = 240$, diameter 1.366 nm), along a graphene nanoribbon of width 19.001 nm located along the x axis in the xy plane (the zig-zag direction of the nanoribbon coincides with the x axis, the armchair direction coincides with the y axis). The gray color marks the surface of the flat substrate at $z = 0$ on which the graphene nanoribbon lies.

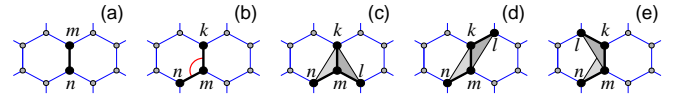


FIG. 2: (Color online) Configurations containing up to i th type of nearest-neighbor interactions for (a) $i = 1$, (b) $i = 2$, (c) $i = 3$, (d) $i = 4$, and (e) $i = 5$.

where $\epsilon_1 = 4.9632 \text{ eV}$ is the energy of the valence bond and $\rho_0 = 1.418 \text{ \AA}$ is the equilibrium length of the bond; the potential of the valence angle

$$U_2(\mathbf{u}_1, \mathbf{u}_2, \mathbf{u}_3) = \epsilon_2 (\cos \varphi - \cos \varphi_0)^2, \quad (4)$$

$$\cos \varphi = (\mathbf{u}_3 - \mathbf{u}_2, \mathbf{u}_1 - \mathbf{u}_2) / (|\mathbf{u}_3 - \mathbf{u}_2| \cdot |\mathbf{u}_2 - \mathbf{u}_1|),$$

so that the equilibrium value of the angle is defined as $\cos \varphi_0 = \cos(2\pi/3) = -1/2$; the potential of the torsion angle

$$U_i(\mathbf{u}_1, \mathbf{u}_2, \mathbf{u}_3, \mathbf{u}_4) = \epsilon_i (1 + z_i \cos \phi), \quad (5)$$

$$\cos \phi = (\mathbf{v}_1, \mathbf{v}_2) / (|\mathbf{v}_1| \cdot |\mathbf{v}_2|),$$

$$\begin{aligned}\mathbf{v}_1 &= (\mathbf{u}_2 - \mathbf{u}_1) \times (\mathbf{u}_3 - \mathbf{u}_2), \\ \mathbf{v}_2 &= (\mathbf{u}_3 - \mathbf{u}_2) \times (\mathbf{u}_3 - \mathbf{u}_4),\end{aligned}$$

where the sign $z_i = 1$ for the indices $i = 3, 4$ (equilibrium value of the torsional angle $\phi_0 = \pi$) and $z_i = -1$ for the index $i = 5$ ($\phi_0 = 0$).

The specific values of the parameters are $\alpha_0 = 1.7889 \text{ \AA}^{-1}$, $\epsilon_2 = 1.3143 \text{ eV}$, and $\epsilon_3 = 0.499 \text{ eV}$, they are found from the frequency spectrum of small-amplitude oscillations of a sheet of graphite [35]. According to previous study [36], the energy ϵ_4 is close to the energy ϵ_3 , whereas $\epsilon_5 \ll \epsilon_4$ ($|\epsilon_5/\epsilon_4| < 1/20$). Therefore, in what follows we use the values $\epsilon_4 = \epsilon_3 = 0.499 \text{ eV}$ and assume $\epsilon_5 = 0$, the latter means that we omit the last term in the sum (2). More detailed discussion and motivation of our choice of the interaction potentials (3), (4), (5) can be found in earlier publication [37].

The van der Waals interactions of the carbon atoms of the graphene sheet, flake and fullerene macromolecule with flat substrate are described by the Lennard-Jones (LJ) potential (m, l)

$$W(z) = \epsilon_z [m(z_0/z)^l - n(z_0/z)^m] / (l - m), \quad (6)$$

where z is the distance from carbon atom to the outer surface of the substrate, which is the plane $z = 0$. Potential $W(z)$ in Eq. (6) is the interaction energy of a carbon atom as a function of the distance to the substrate. This energy was found numerically for different substrates [38, 39]. The calculations showed that interaction energy with substrate $W(z)$ can be described with a high accuracy by LJ potential (6) with power $l > k$. Potential (6) has the minimum $W(z_0) = -\epsilon_z$ (ϵ_z is the binding energy of the atom with substrate). For the surface of the α -graphite crystal, $\epsilon_z = 0.052 \text{ eV}$, $z_0 = 3.37 \text{ \AA}$, $l = 10$, $m = 3.75$.

Nonvalence interactions of the carbon atoms of the nanoribbon and rectangular flake (fullerene macromolecule) are described by the (6,12) LJ potential

$$V(r) = \epsilon_c \{ [(r_c/r)^6 - 1]^2 - 1 \}, \quad (7)$$

where $\epsilon_c = 0.002757 \text{ eV}$, $r_c = 3.807$ [40].

III. DECELERATION OF NANOPARTICLES IN THE BALLISTIC REGIME OF MOTION

It was shown in the papers [31, 32] that nanoparticles (cluster Au_{459} , buckminsterfullerene C_{60}) moving at high speeds on the surface of a graphene sheet have a new regime of "ballistic" friction, which differs from the well-studied "diffusion" friction arising from the drift of nanoparticles at low speeds. In these regimes, friction is provided by various types of interaction of nanoparticles with the substrate. To explain the mechanism of "ballistic" friction, we will simulate the free motion of carbon nanoparticles (of RGF and SF) along the graphene nanoribbon (GNR) of size $103.0 \times 19.0 \text{ nm}^2$ (number of carbon atoms $N_1 = 75598$) lying on a flat substrate.

Let the substrate on which the nanoribbon lies coincide with the plane $z = 0$ (nanoribbon plane coincides with the plane $z = z_0$) and let the nanoribbon lie along the axis x . We place a carbon nanoparticle (RGF or SF) on the center line at the left edge of the nanoribbon – see Fig. 1. To obtain a normalized state of the molecular system RGF(SF)/GNR, we will place it in a Langevin thermostat. To do this, we will fix the coordinates x, y of the carbon atoms from the lower left and upper right corners of the nanoribbon (we put the velocities $\dot{x}_n \equiv 0$, $\dot{y}_n \equiv 0$ for $n = 1, N_1$). In order to avoid nanoparticle motion during the thermalization of the system, we will also fix these coordinates for two opposite angular atoms of RGF and for one atom of SF. Next, we numerically integrate the Langevin system of equations

$$M_n \ddot{\mathbf{u}}_n = -\frac{\partial H}{\partial \mathbf{u}_n} - \Gamma M_n \dot{\mathbf{u}}_n + \Xi_n, \quad n = 1, \dots, N, \quad (8)$$

where damping coefficient $\Gamma = 1/t_r$ (time $t_r = 0.4 \text{ ps}$ characterizes the intensity of energy exchange with the thermostat) and $\Xi_n = \{\xi_{n,i}\}_{i=1}^3$ is three-dimensional vector of normally distributed random forces (white noise) normalized by conditions

$$\langle \xi_{n,i}(t_1) \xi_{m,j}(t_2) \rangle = 2M_n \Gamma k_B T \delta_{nm} \delta_{ij} \delta(t_2 - t_1)$$

(T is thermostat temperature, k_B is Boltzmann constant).

Let us take the initial conditions which correspond to the ground stationary state of the molecular system "nanoparticle/nanoribbon" and numerically integrate the Langevin system of equations (8) during the time $t_0 = 20t_r$. For this time, the system will come into full equilibrium with the thermostat, and we will have its thermalized state

$$\{\mathbf{w}_n = \mathbf{u}_n(t_0), \quad \mathbf{v}_n = \dot{\mathbf{u}}_n(t_0)\}_{n=1}^N.$$

To simulate the free motion of a nanoparticle along a thermalized infinite graphene nanoribbon, we leave the interaction with the thermostat only for the nanoribbon atoms located at a distance less than 1 nm from its left or right edge. Let us remove all the fixation conditions for the nanoparticle atoms and give them the additional initial velocity $v_0 = 500 \text{ m/s}$ directed along the x axis. To do this, we will numerically integrate the system of equations of motion

$$M_n \ddot{\mathbf{u}}_n = -\frac{\partial H}{\partial \mathbf{u}_n} - \Gamma M_n \dot{\mathbf{u}}_n + \Xi_n, \quad (9)$$

$$1 \leq n \leq N_t, \quad N_1 - N_t < n \leq N_1,$$

$$M_n \ddot{\mathbf{u}}_n = -\frac{\partial H}{\partial \mathbf{u}_n}, \quad (10)$$

$$N_t < n \leq N_1 - N_t, \quad N_1 < n \leq N$$

with initial conditions

$$\mathbf{u}_n(0) = \mathbf{w}_n, \quad \dot{\mathbf{u}}_n(0) = \mathbf{v}_n, \quad n = 1, \dots, N_1, \quad (11)$$

$$\mathbf{u}_n(0) = \mathbf{w}_n, \quad \dot{\mathbf{u}}_n(0) = \mathbf{v}_n + v_0 \mathbf{e}_x, \quad n = N_1 + 1, \dots, N,$$

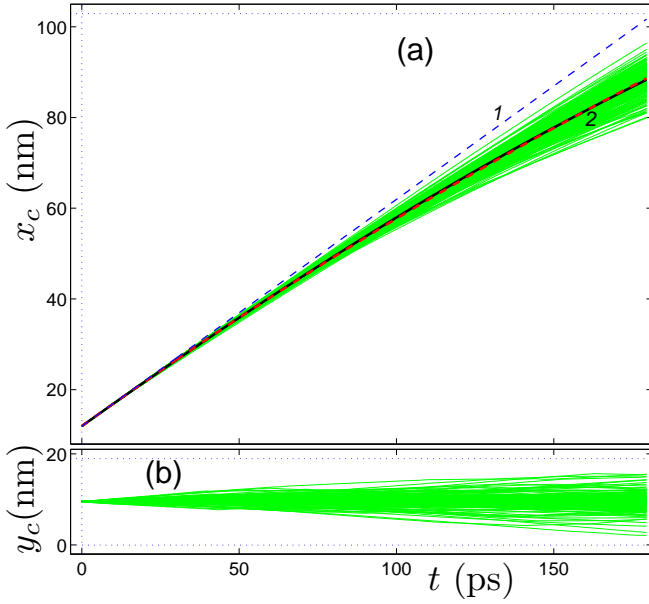


FIG. 3: Trajectories of movement of the center of gravity of RGF of size 3.56×3.26 (number of atoms $N_2 = 478$) along GNR of size 103×19 nm² (the number of atoms $N_1 = 75598$) at a temperature $T = 300$ K (initial velocity $v_0 = 500$ m/s). The green curves show the trajectories of motion for 256 independent realizations of the initial thermalization of the system, the dashed line 1 is the trajectory for motion with constant velocity $v = v_0$, the black curve 2 is the averaged trajectory $\bar{x}_c(t)$, and the dashed red curve is the trajectory of motion (12) with the coefficient of friction $\gamma = 1.80$ ns⁻¹. Part (a) shows the dependence of the x coordinate of the center of gravity x_c on time t , part (b) shows the dependence on time for coordinate y_c . Horizontal dotted lines show the boundaries of the nanoribbon.

where the number of edge atoms of the nanoribbon interacting with the thermostat is $N_t = 900$, the vector is $\mathbf{e}_x = (1, 0, 0)$.

Let us follow the movement of the center of gravity of the nanoparticle along the nanoribbon

$$x_c = \frac{1}{N_2} \sum_{n>N_1} x_n, \quad y_c = \frac{1}{N_2} \sum_{n>N_1} y_n.$$

The typical character of the nanoparticle motion is shown in Fig. 3. As can be seen in the figure, the type of trajectory $x_c(t)$ depends on the realization of the initial thermalized state of the system, but interaction with the substrate always leads to a deceleration of the directional movement of the nanoparticle. If the trajectory is averaged over all independent realizations of the thermalized state of the system (if we take the average value $\bar{x}_c(t) = \langle x_c(t) \rangle$), the dynamics can be described with high accuracy as the motion of a particle in a viscous medium:

$$\bar{x}_c(t) = \bar{x}_c(0) + v_0[1 - \exp(-\gamma t)]/\gamma, \quad (12)$$

with the coefficient of viscous "friction" $\gamma > 0$ (the inverse value γ^{-1} corresponds to the time during which

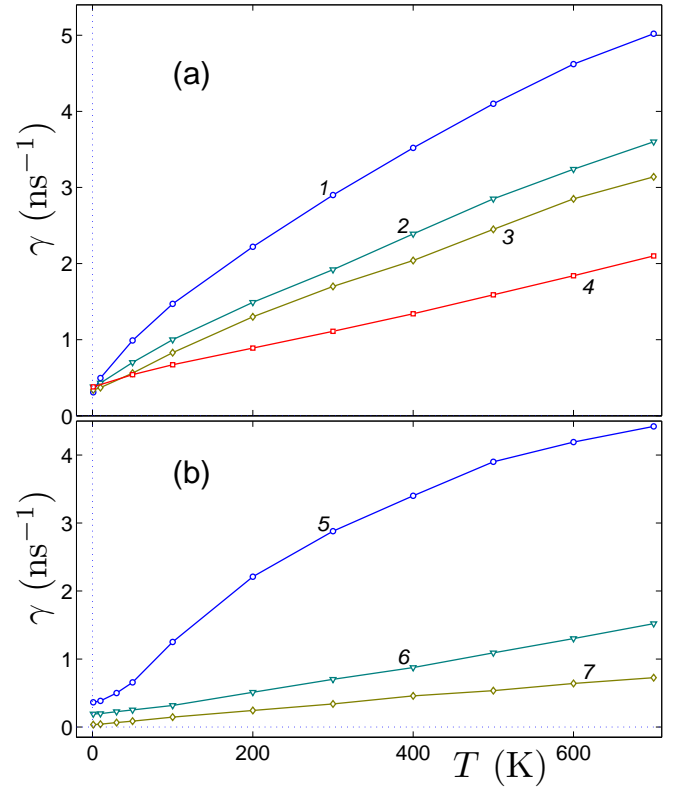


FIG. 4: Dependence of the coefficient of effective friction with substrate γ on temperature T for (a) RGF of size: 0.860×0.709 , 1.842×1.560 , 3.561×3.261 and 7.245×6.665 nm² (curves 1, 2, 3 and 4) and for (b) SF C₂₀, C₆₀ and C₂₄₀ (curves 5, 6 and 7).

the initial velocity of the nanoparticle decreases ϵ times). So for RGF of size 3.56×3.26 nm² at a temperature of $T = 300$ K, the coefficient of friction for motion along a graphene sheet $\gamma = 1.80$ ns⁻¹ – see Fig. 3. In numerical simulation, the averaging of the trajectory was carried out over 256 independent realizations of the initial thermalized state of the system.

Numerical simulation of nanoparticle dynamics has shown that in ballistic regime viscous deceleration (12) occurs at all nanoparticle sizes and temperatures $T \geq 100$ K, but the value of the effective friction coefficient γ depends on the temperature, size and type of nanoparticle – see Fig. 4. The coefficient of friction monotonically increases with the increase in temperature and decreases with the increase in nanoparticle size. For large nanoparticles, the coefficient of friction increases linearly with the increase in temperature. This allows us to conclude that the deceleration of the ballistic motion of nanoparticles is caused by their interaction with the thermal vibrations of the substrate. It should be noted that the "diffusion" regime of nanoparticle motion is characterized by a decrease in friction with an increase in temperature, due to additional thermal activation of their jumps through local energy barriers [41].

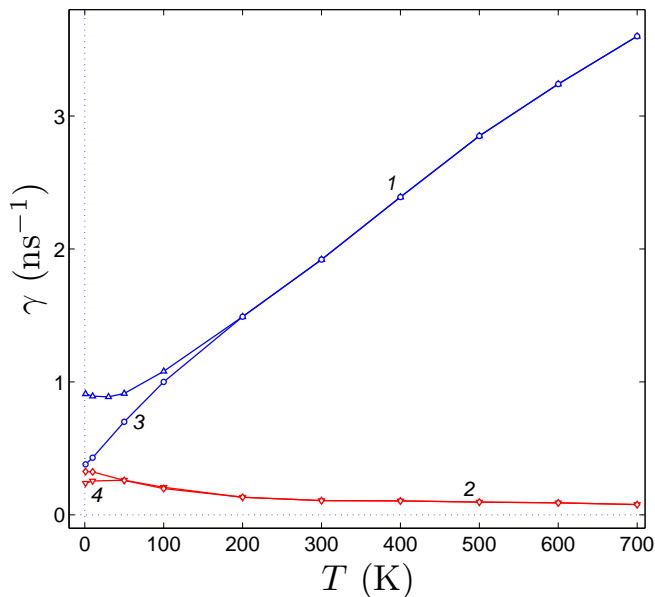


FIG. 5: Dependence of the effective coefficient of friction with the substrate γ on temperature T for RGF of size $1.842 \times 1.560 \text{ nm}^2$ by taking into account all three-dimensional movements of atoms (curves 1, 3) and by taking into account only movements in the xy plane (curves 2, 4). Curves 1, 2 show dependencies by choosing the direction of GRF movement which is commensurate with substrate. Curves 3 and 4 illustrate dependencies by choosing incommensurate direction of GRF movement.

For the diffusion of RGF on a graphene layer, the transitions of the flake from commensurate to incommensurate states with the layer are very important [42, 43]. Let us estimate the contribution of these transitions to friction for the ballistic regime of RGF motion. In our numerical simulation, the zigzag graphene nanoribbon model an infinite graphene layer. Zigzag directions of GNR and RGF coincide with the x axis. Therefore, by shifting the flake along the y axis, we can obtain both directions of RGF movement that are commensurate and incommensurate to the substrate.

Numerical simulation of the motion of a graphene flake of size $1.842 \times 1.560 \text{ nm}^2$ has shown that the choice of a commensurate direction leads to an increase in the coefficient of friction only at low temperatures $T < 100\text{K}$ – see Fig. 5. At higher temperatures, the commensurability of the direction of the flake ballistic movement to the graphene layer does not affect the value of the coefficient of friction. Here, an increase in temperature leads to a monotonous, almost linear, increase in friction.

If, when modeling the ballistic movement of a flake, extra-plane displacements of atoms are prohibited, i.e. if we switch from a three-dimensional to a two-dimensional model, the value of friction will decrease by one order of magnitude and the direction of the temperature dependence of the friction coefficient will change on opposite. When using a 2D model for the ballistic regime, as well

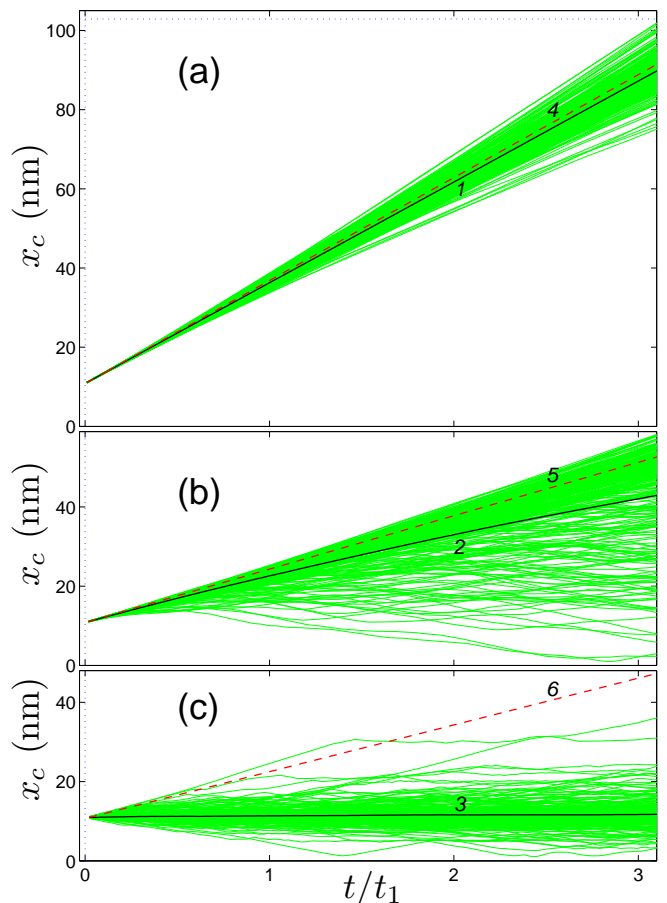


FIG. 6: Trajectories of movement of the mass center of RGF of size $1.842 \times 1.560 \text{ nm}^2$ ($N_2 = 126$) under the action of constant force $F = F_c/N_2$ at (a) $F_c = 0.00045$, (b) 0.00025 and (c) 0.0001 eV/\AA (temperature $T = 100\text{K}$, time $t_1 = 100, 92.9$ and 200 ps). The green curves show the trajectories of motion for 256 independent realizations of the initial thermalization of the system, the black curves 1, 2, 3 are averaged trajectories $\bar{x}_c(t)$, dashed lines 4, 5, 6 are trajectories for motion with constant velocity $v_0 = N_2 F/M_c \gamma$, where the coefficient of friction for ballistic regime of motion $\gamma = 0.00108 \text{ ps}^{-1}$.

as for the diffusion regime of motion, the coefficient of friction will decrease monotonically with the increase in temperature – see Fig. 5. Therefore, it can be concluded that the friction in the ballistic regime of motion has a wave nature. The reason for the deceleration is the interaction of a moving nanoparticle with thermal out-of-plane bending vibrations of a graphene sheet. The greater are these fluctuations, the greater is the value of the coefficient of friction.

Let us note that for a rectangular flake, the initial sliding velocity above the used value $v_0 = 500 \text{ m/s}$ can be obtained as a result of it partially shift beyond the edge of the substrate. Then the return of the flake onto the substrate will lead to its sliding at velocity $v = 600 \text{ m/s}$ [43].

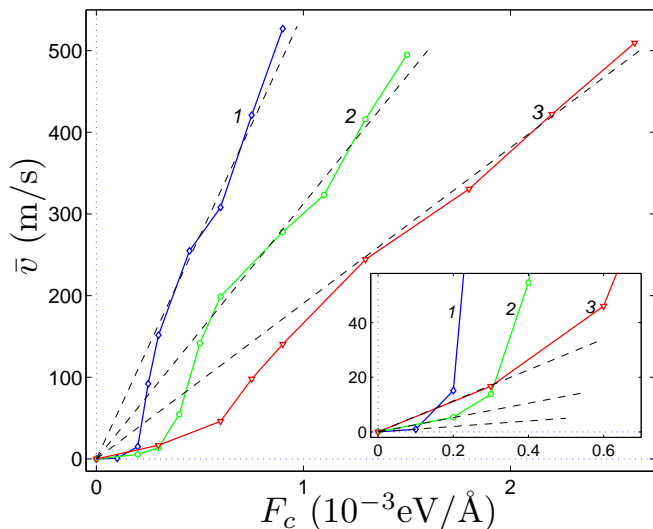


FIG. 7: Dependence of the average value of the velocity of the nanoparticle \bar{v} on the force F_c for RGF of size 1.842×1.560 nm² at a temperature $T = 100, 300$ and 600 K (curves 1, 2 and 3). The dashed lines show the dependencies corresponding to the mobility of the nanoparticle in the ballistic and diffusion (in the inset) regimes of motion.

IV. MOBILITY OF NANOPARTICLES

If a particle of mass M_c moves in a viscous medium along the x axis under the action of an external force F_c , then its dynamics is described by the equation of motion

$$M_c \ddot{x}_c = -\gamma M_c \dot{x}_c + F_c, \quad (13)$$

where γ is the coefficient of friction characterizing the viscosity of the medium. From the equation (13) follows that over time the particle will always enter the regime of motion with a constant velocity $v(F_c) = F_c/\gamma M_c$. Here, the mobility of the nanoparticle, the ratio of the constant velocity of its movement to the force,

$$\mu = v(F_c)/F_c = 1/\gamma M_c \quad (14)$$

completely determines the coefficient of friction γ .

Let us find the mobility of a carbon nanoparticle on a graphene sheet μ through direct modeling of its motion on thermalized sheet under the action of a constant force $F > 0$ applied to each atom of the nanoparticle parallel to the x axis. In this case, the dynamics of the particle will be described by a system of equations of motion

$$M_n \ddot{\mathbf{u}}_n = -\frac{\partial H}{\partial \mathbf{u}_n} + F \mathbf{e}_x, \quad N_1 < n \leq N. \quad (15)$$

The total mass of the particle is $M_c = \sum_{n=1}^{N_2} M_{N_1+n}$, the total force acting on its center of gravity is $F_c = N_2 F$, so we should expect that the velocity of a uniform motion of the particle $v_0(F) = N_2 F/M_c \gamma$. Thus, to simulate

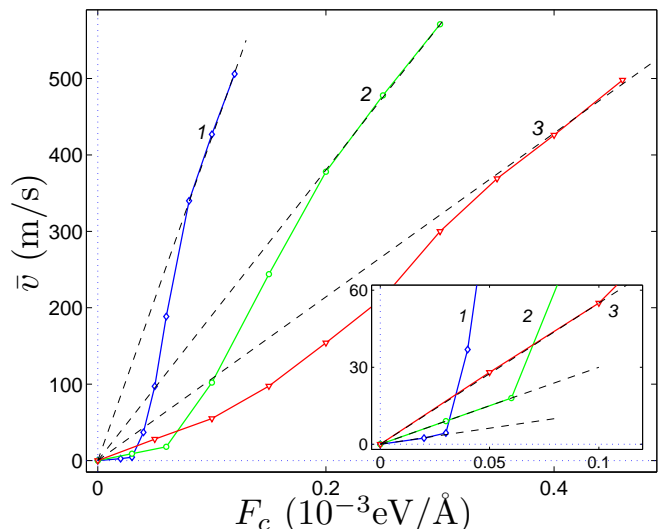


FIG. 8: Dependence of the average value of the velocity of the nanoparticle \bar{v} on the force F_c for SF C₆₀ at a temperature $T = 100, 300$ and 600 K (curves 1, 2 and 3). The dashed lines show the dependencies corresponding to the mobility of the nanoparticle in the ballistic and in the diffusion (in the inset) regimes of motion.

the forced motion of a nanoparticle, it is necessary to numerically integrate the system of equations of motion (9), (10), (15) with an initial condition (11), where the velocity of the initial motion $v_0 = N_2 F/M_c \gamma$.

In the simulation, the trajectory of the particle's center of gravity was averaged over 256 independent realizations of the initial thermalized state of the system $\{\mathbf{w}_n, \mathbf{v}_n\}_{n=1}^N$, and the value of the constant velocity of movement \bar{v} was determined from this trajectory. A form of the trajectories of the nanoparticle motion under the action of a constant force is shown in Fig. 6. Numerical simulation has shown that the nanoparticle has two values of mobility μ . At high values of the external force, the particle always enters the ballistic regime of motion with constant velocity $\bar{v} \approx v_0(F)$ – see Fig. 6 (a). Here the mobility is $\mu \approx 1/M_c \gamma$, where γ is the coefficient of friction for ballistic regime of motion. At small values of force, the particle always enters the diffusion regime of motion with average velocity value $\bar{v} \ll v_0(F)$ – see Fig. 6 (c). At intermediate values of force, both diffusive and ballistic motion of the particle is possible – see Fig. 6 (b).

The ballistic mobility of a nanoparticle always significantly exceeds the diffusion mobility. For example, for RGF of size 1.842×1.560 nm² (for fullerene C₆₀) at a temperature $T = 100$ K, mobility for the ballistic regime exceeds that for the diffusion regime of motion by 60 (35) times, at $T = 300$ K by 12 (5.2) times, and at $T = 600$ K by 3.5 (1.9) times.

The form of the dependence of the average value of the nanoparticle velocity \bar{v} on the value of the con-

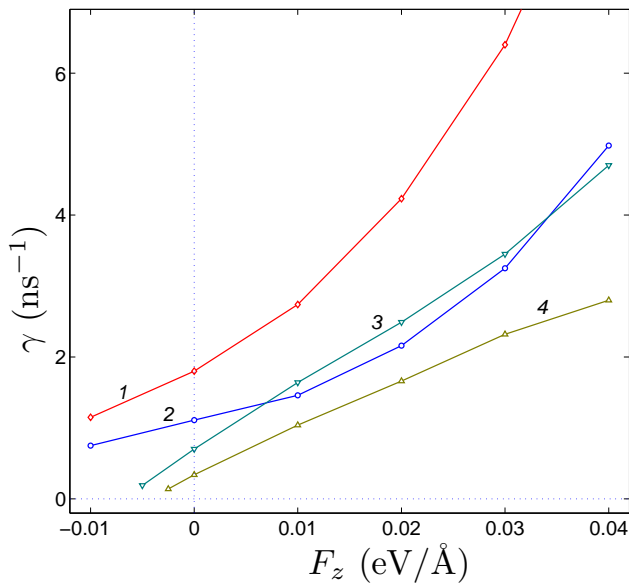


FIG. 9: Dependence of the coefficient of effective friction with the substrate γ on the force of the normal load F_z for ballistic motion of RGF of size: 3.561×3.261 , 7.245×6.665 nm² (curves 1, 2) and of SF C₆₀, C₂₄₀ (curves 3, 4). Temperature $T = 300$ K.

stant force F_c is shown in Fig. 7 and 8. The velocity value always monotonically increases with the increase in force. For high and low values of force, the velocity of motion becomes directly proportional to the force: for small values $\bar{v} \sim \mu_d F_c$, and for large values $\bar{v} \sim \mu_b F_c$ with proportionality coefficients $\mu_d \ll \mu_b$ (μ_d and μ_b is the mobility of the particle in diffusion and ballistic regimes of motion). Thus, the simulation shows that in both regimes the particle motion is realized in a viscous medium, but with different coefficients of friction. In the diffusion mode, the effective friction caused by the interaction of the nanoparticle with the substrate is significantly higher than the friction in the ballistic mode: $\gamma_d = 1/M_c \mu_d \gg \gamma_b = 1/M_c \mu_b$.

With the increase in temperature, friction decreases monotonically in the diffusion regime, and it increases in the ballistic regime of motion, which indicates different mechanisms of its occurrence. Therefore, the difference between the diffusion and ballistic regimes of motion is most pronounced at low temperatures. The simulation shows that at speed of motion $v < 10$ m/s the nanoparticle always enters the diffusion regime and at $v > 100$ m/s – the ballistic regime of motion.

V. EFFECT OF NORMAL LOAD ON FRICTION

According to the empirical Amonton-Coulomb law, the friction force increases with the increase in the normal load. Recent papers [30, 44–46] have shown that for layered structures such as graphite, this law may not be

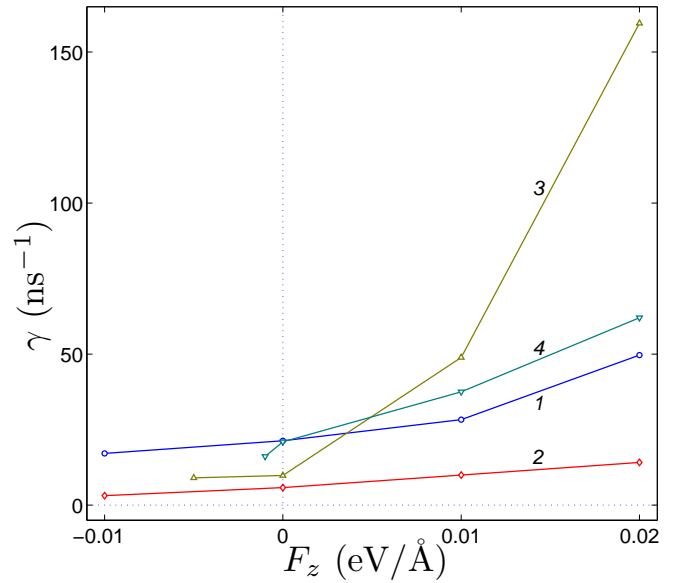


FIG. 10: Dependence of the coefficient of effective friction with the substrate γ on the force of the normal load F_z for diffusive motion of RGF of size: 1.84×1.56 , 3.561×3.261 (curves 1, 2) and for SF C₆₀, C₂₄₀ (curves 3, 4). Temperature $T = 300$ K.

fulfilled at the nanoscale. An increase in the normal load can lead to a decrease in the friction force between the layers.

Let us check the Amonton-Coulomb law for nanoparticles located on a graphene sheet. For this, we will simulate their movement taking into account a force F_z that presses it vertically to the substrate. In this case, the dynamics of the nanoparticle will be described by a system of equations of motion

$$M_n \ddot{\mathbf{u}}_n = -\frac{\partial H}{\partial \mathbf{u}_n} + F_z \mathbf{e}_z, \quad N_1 < n \leq N, \quad (16)$$

where vector $\mathbf{e}_z = (0, 0, 1)$. Thus, to simulate the ballistic motion of a nanoparticle taking into account a normal load F_z , it is necessary to numerically integrate a system of equations of motion (9), (10), (16) with an initial condition (11), where the velocity $v_0 = 500$ m/s.

Numerical simulation of dynamics has shown that the addition of a normal force F_z pressing the nanoparticle to the substrate leads to a monotonous increase in the coefficient of friction γ in both ballistic and diffusion regimes of motion – see Fig. 9, 10. The rate of growth of the coefficient of friction decreases with the increase in particle size. Thus, for the nanoparticles considered in this paper, the Amonton-Coulomb law is fulfilled.

It is not yet possible to verify the validity of the law for large nanoparticles using a full-atom model due to computational difficulties associated with very large dimensions of systems of equations of motion. However this can be done if, instead of a 3D model, we use a 2D model that requires significantly less computing re-

sources. It has been shown by using this model [47] that by ballistic motion of large graphene flakes, the friction force acts differently on the edge and on the inner atoms of the flake. For the edges of the flake, friction always increases with an increase in the normal load due to the indentation of the edges into the substrate, and for the inner part, friction decreases due to additional alignment of the surfaces of the flake and the substrate. The inner sections will make the main contribution to friction only for flakes of size $L > 250$ nm, therefore, only for flakes of this large size should we expect a decrease in friction with an increase in normal load.

VI. CONCLUSION

The numerical simulation of motion of carbon nanoparticles (rectangular graphene flakes, spherical fullerenes) on the surface of a graphene sheet lying on a flat substrate has shown that there are two regimes of friction: diffusion and ballistic. In these regimes, effective friction takes place due to different types of interaction of the nanoparticle with a graphene sheet. In the well-studied diffusion regime (for velocities $v < 10$ m/s), friction occurs due to overcoming local energy barriers. Here, the value of friction depends on the commensurability of the direction of motion of the nanoparticle with the lattice of the sheet, and the friction coefficient always decreases monotonically with the increase in temperature. In the ballistic regime (for $v > 100$ m/s), the commensurability of the direction of motion does not affect on friction,

and the friction coefficient increases monotonically, almost linearly, with the increase in temperature. Here, the friction is of a wave nature. The cause of deceleration is the interaction of a moving nanoparticle with thermal out-of-plane bending vibrations of a graphene sheet (the greater are these vibrations, the higher is the friction).

Simulation of the motion of nanoparticles under the action of a constant force has shown that their mobility in the ballistic regime (at large values of force) is higher than in the diffusion regime (at small values of force). With an increase in temperature in the diffusion regime, the mobility monotonically increases, and it decreases in the ballistic regime. Therefore, the difference between the diffusion and ballistic regimes of motion is most pronounced at low temperatures.

The simulation of motion in the presence of a normal force pressing the nanoparticle to the substrate has shown that the increase in the normal load leads to a monotonous increase in the coefficient of friction in both ballistic and diffusion regimes of motion. The rate of growth of the coefficient of friction decreases with increasing particle size, but it always remains positive. It can be concluded that for particles with sizes $L < 10$ nm located on a graphene sheet, the empirical Amonton-Coulomb law is always valid (the violation of the law should be expected for particles of size $L > 250$ nm).

ACKNOWLEDGMENTS

Computational facilities were provided by the Interdepartmental Supercomputer Center of the Russian Academy of Sciences.

-
- [1] K. S. Novoselov, A. K. Geim, S. V. Morozov, D. Jiang, Y. Zhang, S. V. Dubonos, I. V. Grigorieva and A. A. Firsov, Electric Field Effect in Atomically Thin Carbon Films. *Science* **306**(5696), 666-669 (2004).
 - [2] A. H. Castro Neto, F. Guinea, N. M. R. Peres, K. S. Novoselov and A. K. Geim, The electronic properties of graphene. *Rev. Mod. Phys.* **81**, 109-162 (2009).
 - [3] E. Koren, I. Leven, E. Lörtscher, A. Knoll, O. Hod and U. Duerig, Coherent commensurate electronic states at the interface between misoriented graphene layers. *Nature Nanotech.* **11**, 752-757 (2016).
 - [4] J. C. Meyer, A. K. Geim, M. Katsnelson, K. Novoselov, T. Booth and S. Roth, The structure of suspended graphene sheets. *Nature* **446**, 60-63 (2007).
 - [5] C. Lee, X. Wei, J. W. Kysar and J. Hone, Measurement of the Elastic Properties and Intrinsic Strength of Monolayer Graphene. *Science* **321**, 385-388 (2008).
 - [6] A. Falin, Q. Cai, E. J. G. Santos, D. Scullion, D. Qian, R. Zhang, Z. Yang, S. Huang, K. Watanabe, T. Taniguchi, M. R. Barnett, Y. Chen, R. S. Ruoff and L. H. Li, Mechanical properties of atomically thin boron nitride and the role of interlayer interactions. *Nat. Commun.* **8**, 15815 (2017).
 - [7] E. Han, J. Yu, E. Annevelink, J. Son, D. A. Kang, K. Watanabe, T. Taniguchi, E. Ertekin, P. Y. Huang and A. M. van der Zande, Ultrasoft slip-mediated bending in few-layer graphene. *Nature Materials* **19**, 305-309 (2020).
 - [8] P. E. Sheehan and C. M. Lieber, Nanotribology and nanofabrication of MoO₃ structures by atomic force microscopy. *Science* **272**, 1158-1161 (1996).
 - [9] M. Dienwiebel, G. S. Verhoeven, N. Pradeep, J. W. Frenken, J. A. Heimberg and H. W. Zandbergen, Superlubricity of graphite. *Phys. Rev. Lett.* **92**, 126101 (2004).
 - [10] C. Lee, Q. Li, W. Kalb, X.-Z. Liu, H. Berger, R. W. Carpick and J. Hone, Frictional characteristics of atomically thin sheets. *Science* **328**, 76-80 (2010).
 - [11] S. Cahangirov, C. Ataca, M. Topsakal, H. Sahin and S. Ciraci, Frictional figures of merit for single layered nanostructures. *Phys. Rev. Lett.* **108**, 126103 (2012).
 - [12] Z. Liu, J. Yang, F. Grey, J. Z. Liu, Y. Liu, Y. Wang, Y. Yang, Y. Cheng and Q. Zheng, Observation of microscale superlubricity in graphite. *Phys. Rev. Lett.* **108**, 205503 (2012).
 - [13] J. Yang, Z. Liu, F. Grey, Z. Xu, X. Li, Y. Liu, M. Urbakh, Y. Cheng and Q. Zheng, Observation of high-speed microscale superlubricity in graphite. *Phys. Rev. Lett.* **110**, 255504 (2013).
 - [14] E. Koren, E. Lörtscher, C. Rawlings, A. W. Knoll and U. Duerig, Adhesion and friction in mesoscopic graphite contacts. *Science* **348**, 679-683 (2015).

- [15] I. Leven, D. Krepel, O. Shemesh, and O. Hod, Robust Superlubricity in Graphene/h-BN Heterojunctions. *J. Phys. Chem. Lett.* **4**, 115-120 (2013).
- [16] A. Geim and I. Grigorieva, Van der Waals heterostructures. *Nature* **499**, 419-425 (2013).
- [17] K. S. Novoselov, A. Mishchenko, A. Carvalho and A. H. Castro Neto, 2D materials and van der Waals heterostructures. *Science* **353**(6298), 461 (2016).
- [18] C. R. Woods, L. Britnell, A. Eckmann, R. S. Ma, J. C. Lu, H. M. Guo, X. Lin, G. L. Yu, Y. Cao, R. V. Gorbachev, A. V. Kretinin, J. Park, L. A. Ponomarenko, M. I. Katsnelson, Y. N. Gornostyrev, K. Watanabe, T. Taniguchi, C. Casiraghi, H. J. Gao, A. K. Geim and K. S. Novoselov, Commensurate-incommensurate transition in graphene on hexagonal boron nitride. *Nature Phys.* **10**, 451-456 (2014).
- [19] G. J. Slotman, M. M. van Wijk, P. L. Zhao, A. Fasolino, M. I. Katsnelson and S. Yuan, Effect of Structural Relaxation on the Electronic Structure of Graphene on Hexagonal Boron Nitride. *Phys. Rev. Lett.* **115**, 186801 (2015).
- [20] D. Mandelli, I. Leven, O. Hod and M. Urbakh, Sliding friction of graphene/hexagonal-boron nitride heterojunctions: a route to robust superlubricity. *Sci. Rep.* **7**(1), 10851 (2017).
- [21] J. A. Williams and H. R. Le, Tribology and MEMS. *J. Phys. D: Appl. Phys.* **39**, R201-R214 (2006).
- [22] K. Shinjo and M. Hirano, Dynamics of friction: superlubric state. *Surface Science* **283**, 473-478 (1993).
- [23] O. Hod, E. Meyer, Q. Zheng, and M. Urbakh, Structural superlubricity and ultralow friction across the length scales *Nature (London)* **563**, 485 (2018).
- [24] J. M. Martin and A. Erdemir, Superlubricity: Friction's vanishing act. *Phys. Today* **71**, No. 4, 40 (2018).
- [25] M. Z. Baykara, M. R. Vazirisereshk, and A. Martini, Emerging superlubricity: A review of the state of the art and perspectives on future research. *Appl. Phys. Rev.* **5**, 041102 (2018).
- [26] D. Berman, A. Erdemir, and A. V. Sumant, Approaches for Achieving Superlubricity in Two-Dimensional Materials. *ACS Nano* **12**, 2122 (2018).
- [27] Y. Song, D. Mandelli, O. Hod, M. Urbakh, M. Ma, and Q. Zheng, Robust microscale superlubricity in graphite/hexagonal boron nitride layered heterojunctions. *Nat. Mater.* **17**, 894 (2018).
- [28] W. Ouyang, D. Mandelli, M. Urbakh, and O. Hod, Nanoserpents: Graphene Nanoribbons Motion on Two-Dimensional Hexagonal Materials. *Nano Lett.* **18**(9), 6009-6016 (2018).
- [29] A. Vanossi, N. Manini, M. Urbakh, S. Zapperi, and E. Tosatti, Colloquium: Modeling friction: From nanoscale to mesoscale. *Rev. Mod. Phys.* **85**, 529 (2013).
- [30] D. Mandelli, W. Ouyang, O. Hod, and M. Urbakh, Negative Friction Coefficients in Superlubric Graphite-Hexagonal Boron Nitride Heterojunctions. *Phys. Rev. Lett.* **122**, 076102 (2019).
- [31] R. Guerra, U. Tartaglino, A. Vanossi, and E. Tosatti. Ballistic nanofriction. *Nature Mater* **9**, 634-637 (2010).
- [32] M. Jafary-Zadeh, C.D. Reddy, V. Sorkin, and Y.-W. Zhang. Kinetic nanofriction: a mechanism transition from quasi-continuous to ballistic-like Brownian regime. *Nanoscale Research Letters* **7**, 148 (2012).
- [33] D.W. Noid, B.G. Sumpter, and B. Wunderlich. Molecular dynamics simulation of twist motion in polyethylene. *Macromolecules* **24**(14), 4148-4151 (1991).
- [34] B.G. Sumpter, D.W. Noid, G.L. Liang, and B. Wunderlich. Atomistic dynamics of macromolecular crystals. *Adv. Polym. Sci.* **116**, 27 (1994).
- [35] A.V. Savin and Yu.S. Kivshar. Discrete breathers in carbon nanotubes. *Europhys. Letters* **82**, 66002 (2008).
- [36] D. Gunlycke, H.M. Lawler, and C.T. White. Lattice vibrations in single-wall carbon nanotubes. *Phys. Rev. B* **77**, 014303 (2008).
- [37] A.V. Savin, Yu.S. Kivshar, and B. Hu. Suppression of thermal conductivity in graphene nanoribbons with rough edges. *Phys. Rev. B* **82**, 195422 (2010).
- [38] A.V. Savin, E.A. Korznikova, and S.V. Dmitriev. Dynamics of surface graphene ripplons on a flat graphite substrate. *Phys. Rev. B* **99**, 235411 (2019).
- [39] A.V. Savin. Eigenmodes and resonance vibrations of graphene nanomembranes. *Phys. Rev. B*, **103**, 195435 (2021).
- [40] R. Setton. Carbon nanotubes-II. Cohesion and formation energy of cylindrical nanotubes. *Carbon*, **34**(1), 69-75 (1996).
- [41] L. Prandtl. Ein Gedankenmodell zur kinetischen Theorie der festen Körper. *Z. Angew. Math. Mech.* **8**, 85 (1928).
- [42] I.V. Lebedeva, A.A. Knizhnik, A.M. Popov, O.V. Ershova, Y.E. Lozovik, and B.V. Potapkin. Fast diffusion of a graphene flake on a graphene layer *Phys. Rev. B* **82**, 155460 (2010).
- [43] Y. Liu, F. Grey, and Q. Zheng, The high-speed sliding friction of graphene and novel routes to persistent superlubricity. *Sci Rep* **4**, 4875 (2014).
- [44] Z. Deng, A. Smolyanitsky, Q. Li, X.-Q. Feng, and R.J. Cannara. Adhesion-dependent negative friction coefficient on chemically modified graphite at the nanoscale. *Nature Materials* **11**, 1032-1037 (2012).
- [45] A. Smolyanitsky and J.P. Killgore. Anomalous friction in suspended graphene. *Phys. Rev. B* **86**, 125432 (2012).
- [46] J. Sun, Y. Zhang, Z. Lu, Q. Li, Q. Xue, S. Du, J. Pu, and L. Wang. Superlubricity Enabled by Pressure-Induced Friction Collapse. *J. Phys. Chem. Lett.* **9**, 2554-2559 (2018).
- [47] A. V. Savin. Effective Friction and Mobility of Graphene Nanoparticles (Nanoribbons and Nanotubes) on a Flat Multilayer h-BN Substrate. *J. Exp. Theor. Phys.* **133**, 754-765 (2021).